General Instability and Optimum Design of Grid-Stiffened Spherical Domes

ROBERT F. CRAWFORD* AND DAVID B. SCHWARTZ†
Martin Company, Baltimore, Md.

Differential equations for doubly curved orthotropic shells are derived, and stability solutions for the orthotropic idealization of grid-stiffened spherical domes are presented. It is assumed that linear, small-deflection theory is appropriate. Some evidence in support of that assumption is given. Grid-stiffening proportions are optimized for design application to the spherical common dome problem, and the appropriate size of the spherical segment forming the dome is determined. The efficiency charts developed show that, in practical ranges of application, efficiently designed grid-stiffened domes would weigh only 30–40% of monocoque domes they would replace.

Introduction

COMMON domes between tandem propellant tanks of rocket launch vehicles are required to remain structurally stable when they are acted upon by pressure that tends to collapse them. The use of monocoque common domes would, because of their excessive weight, nullify the advantages of a common dome. Therefore, stiffened common domes for such vehicles as Saturn and post-Saturn are investigated to determine their potential for efficiently meeting the stability requirement.

The structural sandwich concept being used for the common domes in the present Saturn vehicles has several disadvantages: 1) structural reliability of core-to-facing bonds is characteristically low; 2) reliable and leak-resistant joints are difficult to develop; 3) inspection for a leakage into the core is unreliable; and 4) fabrication costs are generally high. These disadvantages of sandwich construction led to the investigation of grid-stiffened domes comprised of only one skin and attached stiffening elements as shown in Fig. 1. This type of construction appears to circumvent some of the disadvantages of sandwich construction.

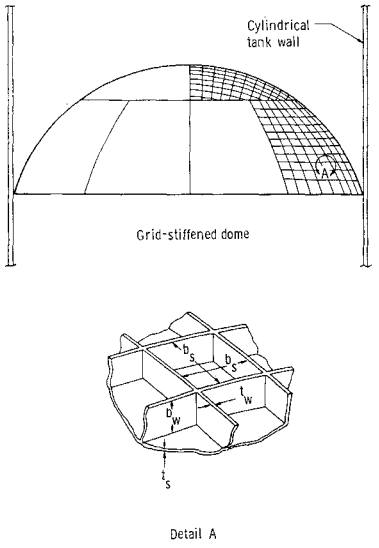

Fig. 1 Spherical common dome with square-grid-stiffening pattern.

Received April 29, 1964; revision received November 12, 1964.
* Senior Staff Engineer, Solid Mechanics Section. Member AIAA.
† Senior Engineering Specialist, Solid Mechanics Section.

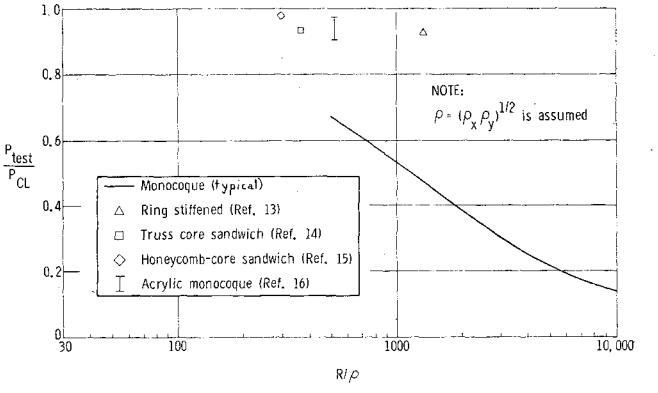

Fig. 2 Ratio of experimental buckling load, P_{test}, to that predicted by classical, small-deflection theory, P_{CL}, vs cylinder radius-to-radius of gyration ratio, R/ρ.

The investigation was done in two parts: 1) derivation and solution of governing differential equations for orthotropic idealization of grid-stiffened spherical domes, and 2) optimization of stiffening and over-all shell proportions for this type of common dome.

Applicability of Linear Theory

Figure 2 shows ratios of experimentally determined axial buckling loads to those predicted by linear, small-deflection theory for a variety of stiffened and monocoque cylindrical shells. The data are plotted against respective ratios of shell radius to radius of gyration. It is evident that close correlation is obtained for the stiffened shells. The monocoque data are included in Fig. 2 to demonstrate the trend, even for monocoque shells, for closer correlation as radius of gyration increases. Donnell and Wan[1] analytically demonstrated this trend by showing that the sensitivity of monocoque shells to given initial imperfections decreases with increasing radius of gyration. Therefore, the stability of stiffened shells with their characteristically greater radii of gyration can be expected to be relatively insensitive to initial imperfections which are known to be so detrimental to the stability of monocoque shells. Thus, it is judged that small-deflection theory should be used in predicting general instability of grid-stiffened spherical domes so long as they are deep and have relatively large radii of gyration.

Stability Analysis

In the following small deflection analysis of doubly curved shells of constant positive curvatures, all terms that would

lead to nonlinearities in the differential equations of equilibrium are neglected. Linear terms of the same type neglected by Donnell[2] are also neglected here. Since the grid-stiffened shell is, in general, high in transverse shearing stiffness, transverse shearing distortions are also neglected.

The following set of three equilibrium equations is similar to those derived by Donnell and can be derived by elementary theory (summing forces and moments in all directions on a distorted differential element of the shell)‡:

$$\frac{\partial^2 M_x}{\partial x^2} + 2\frac{\partial^2 M_{xy}}{\partial x\,\partial y} + \frac{\partial^2 M_y}{\partial y^2} - \frac{N_x}{R_x} - \frac{N_y}{R_y} - \bar{N}_x\frac{\partial^2 w}{\partial x^2} - 2\bar{N}_{xy}\frac{\partial^2 w}{\partial x\,\partial y} - \bar{N}_y\frac{\partial^2 w}{\partial y^2} = 0 \quad (1)$$

$$(\partial N_x/\partial x) + (\partial N_{xy}/\partial y) = 0 \quad (2)$$

$$(\partial N_y/\partial y) + (\partial N_{xy}/\partial x) = 0 \quad (3)$$

The barred forces in Eq. (1) are the prebuckling membrane forces per unit width; only these are assumed to exist in the prebuckled state. The nonbarred forces, M_x, M_{xy}, M_y, N_x, N_{xy}, and N_y, are the incremental changes in the prebuckling state of force which occur during small deflection from the prebuckling equilibrium position per unit width; x and y are orthogonal curvilinear coordinates in the midplane of the unbuckled shell, and z is normal to the prebuckled shell surface; w is the incremental displacement that occurs at buckling in directions normal to the shell's surface; and R_x and R_y are principal radii of curvature in whose planes x and y coordinates lie, respectively.

The force-displacement relationships for an orthotropic shell may be approximated in the following linear form for small-deflection regime:

$$\left.\begin{aligned}
M_x &= D_x\left(\frac{\partial^2 w}{\partial x^2} + \nu_y\frac{\partial^2 w}{\partial y^2}\right)\\
M_y &= D_y\left(\frac{\partial^2 w}{\partial y^2} + \nu_x\frac{\partial^2 w}{\partial x^2}\right)\\
M_{xy} &= D_{xy}\,(\partial^2 w/\partial x\,\partial y)\\
N_x &= E_x\left[\frac{\partial u}{\partial x} + \mu_y\frac{\partial v}{\partial y} - w\left(\frac{1}{R_x} + \frac{\mu_y}{R_y}\right)\right]\\
N_y &= E_y\left[\frac{\partial v}{\partial y} + \mu_x\frac{\partial u}{\partial x} - w\left(\frac{1}{R_y} + \frac{\mu_x}{R_x}\right)\right]\\
N_{xy} &= G_{xy}\,[(\partial u/\partial y) + (\partial v/\partial x)]
\end{aligned}\right\} \quad (4)$$

where

D_x, D_y = flexural stiffnesses in x and y directions, respectively, per unit width
D_{xy} = shell's twisting stiffness per unit width
E_x, E_y = extensional stiffnesses in x and y directions, respectively, per unit width
G_{xy} = in-plane shearing stiffness per unit width
ν_x, ν_y = Poisson ratios associated with flexural distortions
μ_x, μ_y = Poisson ratios associated with extensional distortions
u, v, w = incremental displacements in x, y, and z directions, respectively, which occur during buckling

‡ This analysis does not account for the fact that the stiffening elements being considered are only on one side of the shell and therefore will affect its buckling load. Van der Neut[3] analytically showed some facets of this effect for stiffened cylinders, and Card[4] performed experiments demonstrating that one-sidedness can indeed be significant. A preliminary assessment of the effects of one-sidedness on the present general instability predictions was made after the present work was performed. It shows that the present predictions will be high when the stiffening is on the concave side and low when on the convex side. The discrepancy is expected to be approximately 25% for efficient configurations; however, that quantitative assessment is considered preliminary. Subsequent work should include treatment of one-sidedness.

By expressing Eqs. (1–3) in terms of displacements u, v, and w and combining the resulting three equations to eliminate u and v, a single, eighth-order, linear differential equation in only w is obtained:

$$\nabla_D{}^4\nabla_E{}^4 w + \psi_x\frac{E_y}{E_x}\left(\frac{\partial^4 w}{\partial y^4} + \frac{1}{\delta}\frac{\partial^4 w}{\partial x^2\,\partial y^2}\right) + \psi_y\left(\frac{\partial^4 w}{\partial x^4} + \delta\frac{\partial^4 w}{\partial x^2\,\partial y^2}\right) = \frac{\nabla_E{}^4}{D_x}\left(\bar{N}_x\frac{\partial^2 w}{\partial x^2} + 2\bar{N}_{xy}\frac{\partial^2 w}{\partial x\partial y} + \bar{N}_y\frac{\partial^2 w}{\partial y^2}\right) \quad (5)$$

where

$$\nabla_D{}^4 = \frac{\partial^4}{\partial x^4} + 2\frac{D_3}{D_x}\frac{\partial^4}{\partial x^2\,\partial y^2} + \frac{D_y}{D_x}\frac{\partial^4}{\partial y^4}$$

$$\nabla_E{}^4 = \frac{\partial^4}{\partial x^4} + 2\frac{E_y}{G_3}\frac{\partial^4}{\partial x^2\,\partial y^2} + \frac{E_y}{E_x}\frac{\partial^4}{\partial y^4}$$

$$\psi_x = \frac{E_x}{D_x R_x{}^2}(1 - \mu_x\mu_y) \qquad \psi_y = \frac{E_y}{D_x R_y{}^2}(1 - \mu_x\mu_y)$$

$$\delta = R_y/R_x \qquad D_3 = \nu_x D_y + D_{xy}$$

$$G_3 = \frac{2\,G_{xy}}{1 - \mu_x\mu_y - (2\mu_y G_{xy}/E_y)}$$

For shells that can be represented as orthotropic and of constant double curvature, Eq. (5) may sometimes be used by itself to determine critical forces by simply substituting in it one or more terms of a double sine series expansion of w. That procedure is valid only when either boundary conditions on u, v, and w are satisfied by the expansion used for w or when violation of the actual boundary conditions on u, v, and w have negligible effect. The relationships between u and w and v and w which accompany Eq. (5) are

$$R_x\nabla_E{}^4 u = \left(1 + \frac{\mu_y}{\delta}\right)\frac{\partial^3 w}{\partial x^3} + \frac{E_y}{G_{xy}}\left[1 - \mu_x\mu_y - \frac{1}{\delta}\frac{G_{xy}}{E_x}(1 + \mu_x\delta)\right]\frac{\partial^3 w}{\partial x\,\partial y^2} \quad (6)$$

$$R_y\nabla_E{}^4 v = \frac{E_y}{E_x}(1 + \mu_x\,\delta)\frac{\partial^3 w}{\partial y^3} + \frac{E_y}{G_{xy}}\left[1 - \mu_x\mu_y - \frac{G_{xy}}{E_y}\delta\left(1 + \frac{\mu_y}{\delta}\right)\right]\frac{\partial^3 w}{\partial x^2\,\partial y} \quad (7)$$

It has been shown by Batdorf[5] that, for many practical cases of cylindrical shells, sine series expansions for w may be used in equations similar to Eq. (5) to determine critical loads to close approximations, even when corresponding boundary displacements u and v [Eqs. (6) and (7)] do not agree with the actual ones. No general criterion for neglecting effects of boundary restraint have been developed here; therefore, each situation should be evaluated according to its particular characteristics. It is noted that Eqs. (5–7) reduce to the various monocoque and orthotropic shell small deflection equations that are currently in use for which the same basic assumptions were made.

When Eq. (5) is specialized to the case of a square-grid-stiffened segment of a spherical shell, as shown in Fig. 1, acted upon by uniform pressure, it becomes

$$\nabla_D{}^4\nabla_E{}^4 w + \psi\nabla^4 w = -(pR/2D)\nabla_E{}^4\nabla^2 w \quad (8)$$

since

$$D_x = D_y = D \qquad E_x = E_y = \bar{E} \qquad \mu_x = \mu_y = \mu$$

$$\nu_x = \nu_y = \nu \qquad R_x = R_y = R$$

$$\psi_x = \psi_y = \psi = \bar{E}(1 - \mu^2)/DR^2 \qquad \bar{N}_x = \bar{N}_y = -(pR/2)$$

In Eq. (8), the differential operators have become

$$\nabla_D{}^4 = \frac{\partial^4}{\partial x^4} + 2\frac{D_3}{D}\frac{\partial^4}{\partial x^2\partial y^2} + \frac{\partial^4}{\partial y^4}$$

$$\nabla_E^4 = \frac{\partial^4}{\partial x^4} + 2\frac{\bar{E}}{G_3}\frac{\partial^4}{\partial x^2\,\partial y^2} + \frac{\partial^4}{\partial y^4}$$

$$\nabla^4 = (\nabla^2)^2 = \left(\frac{\partial^2}{\partial x^2} + \frac{\partial^2}{\partial y^2}\right)^2$$

As seen from the wavelength equation and geometric proportions for minimum weight developed later, spherical segment domes having grid-stiffening of efficient proportions will be sufficiently large to contain many buckle wavelengths. The shells may, therefore, be considered "deep." In this event, boundary effects are remote from the greater portion of the shell surface and have negligible effect on the critical buckling pressure. Therefore, the following particular solution to Eq. (8) is used:

$$w = A \sin(\pi x/\lambda_x) \sin(\pi y/\lambda_y) \tag{9}$$

Substituting Eq. (9) in (8) gives

$$\frac{p_{cr}R}{2D(\psi)^{1/2}} = \left(\frac{1}{\psi}\right)^{1/2}\left(\frac{\pi}{\lambda_y}\right)^2\left[\frac{\beta^4 + 2(D_3/D)\beta^2 + 1}{\beta^2 + 1}\right] + (\psi)^{1/2}\left(\frac{\lambda_y}{\pi}\right)^2\left[\frac{\beta^2 + 1}{\beta^4 + 2(\bar{E}/G_3)\beta^2 + 1}\right] \tag{10}$$

where

$$\beta = \lambda_y/\lambda_x$$

Minimizing the buckling pressure p_{cr} in Eq. (10) with respect to the buckle half-wavelength λ_y gives

$$\bar{p}_{cr}{}^2 = \frac{\beta^4 + 2(D_3/D)\beta^2 + 1}{\beta^4 + 2(\bar{E}/G_3)\beta^2 + 1} \tag{11}$$

where

$$\frac{\lambda_y}{\pi} = \left\{\frac{1}{\psi}\left[1 + \frac{D_3}{D}\right]\left[1 + \frac{\bar{E}}{G_3}\right]\right\}^{1/4}$$

and p_{cr} has been normalized to $\bar{p}_{cr}$ by dividing it by the critical buckling pressure of a sphere for which $D_3 = D$ and $\bar{E} = G_3$ as for monocoque or sandwich shell whose critical pressure is the classical one:

$$p_{cr} = 4D(\psi)^{1/2}/R \tag{12}$$

Minimizing $\bar{p}_{cr}$ with respect to β, it is seen that $\beta_{min} = 1$ when $D_3/D < \bar{E}/G_3$ and β = any number when $D_3/D \geq \bar{E}/G_3$. Therefore,

$$\bar{p}_{cr} = 1 \qquad D_3/D \geq \bar{E}/G_3 \tag{13}$$

$$\bar{p}_{cr} = \left(\frac{1 + D_3/D}{1 + \bar{E}/G_3}\right)^{1/2} \qquad \frac{D_3}{D} < \frac{\bar{E}}{G_3} \tag{14}$$

Without being concerned over precise values of D_3/D and $\bar{E}/G_3$ for the open section stiffening under consideration, it can be readily verified that $D_3/D < \bar{E}/G_3$. Equation (14) is therefore used in the following weight minimization analysis.

Minimum Weight Analysis

Optimization of Geometric Proportions of Stiffening Elements

The methods and concepts used in this analysis are typical of those used in Refs. 6–8; optimum proportions are those for which both general and local instability are critical under the applied loading. Accordingly, optimum design of the construction shown in Fig. 1 has proportions for which local instability of both the stiffening elements and the shell elements they bound and general instability of the composite are critical under the applied pressure.

General instability is predicted by Eq. (14) of the previous section. Local instability is predicted by considering the stiffening elements and the shell elements they bound to be flat and simply supported along their common edges (uncoupled). There appears to be no published analysis for critical pressures for these small, adjacent, quasi-square spherical segments. However, effects of curvature on them are expected to be negligible for the small values of b_s/R that are involved here, much as Batdorf[5] showed curvature effects to be small for axially compressed cylindrical elements of small width-to-radius ratios. Local buckling is therefore predicted by the flat plate instability equations of Ref. 9. To make the analysis tractable as well as to add some conservatism, it is assumed, in calculating local instability of the shell elements bounded by the stiffeners, that they are stressed as though only the shell participates in carrying the applied pressure. This assumption adds little conservatism to the shell elements' critical pressure, since their center region can be stressed to that extent. For the same reasons, it is assumed in calculating local instability of the stiffening elements that they are stressed to the extent they would be if the shell and stiffening elements become equally stressed under the applied pressure. The data of Ref. 10 show this assumption to be conservative, but not excessively so.

Finally, it is assumed that there is no coupling between local and general instability, and the analysis is restricted to the elastic regime.

Equation (14) can be expressed in the form

$$\frac{p_{cr_G}}{E} = 4C\left[\frac{\bar{t}}{R}\frac{D}{D_s}\frac{D_s}{ER^3}\left(\frac{1 + D_3/D}{1 + \bar{E}/G_3}\right)\right]^{1/2} \tag{15}$$

where

- C = as yet undetermined reduction factor that may be applied to general instability pressure as predicted by Eq. (15)
- p_{cr_G} = critical pressure for general instability
- E = Young's modulus
- $\bar{t}$ = $t_s[1 + (b_w/b_s)(t_w/t_s)]$ (see Fig. 1 for t_s, t_w, b_s, and b_w)
- $\bar{E}$ = $E\bar{t}/(1 - \mu^2)$
- D_s = shell's flexural stiffness [$D_s = Et_s^3/12(1 - \mu^2)$]

The other symbols were defined previously.

Local instability of the shell can be expressed in the form

$$p_{cr_L}/E = 2k_s\pi^2(R/b_s)^2(D_s/ER^3) \tag{16}$$

where k_s is the stability coefficient and b_s and R are shown in Fig. 1.

The ratios in Eq. (15) are closely approximated by the following formulas when, as in the present case, $(b_s/t_s)^2 \gg 1$, $\nu \approx 0$, and only the skin carries in-plane shear[11]:

$$\frac{D}{D_s} \cong (1 - \mu^2)\left(\frac{b_w}{b_s}\right)^3\frac{t_w}{t_s}\left(\frac{b_s}{t_s}\right)^2\left[\frac{4 + (b_w/b_s)(t_w/t_s)}{1 + (b_w/b_s)(t_w/t_s)}\right] \tag{17}$$

$$\frac{D_3}{D} \cong \nu + \left(\frac{t_s}{b_s}\right)^2\frac{[1 + (t_w/t_s)^3\,(b_w/b_s)][(1 + (b_w/b_s)(t_w/t_s)]}{(b_w/b_s)^3(t_w/t_s)[4 + (b_w/b_s)(t_w/t_s)]} \approx 0 \tag{18}$$

$$\bar{E}/G_3 \cong (1 + \mu)(\bar{t}/t_s) - \mu \tag{19}$$

$$D_s/ER^3 = (t_s/R)^3/12(1 - \mu^2) \tag{20}$$

$$\frac{\bar{t}}{R} = \frac{t_s}{b_s}\frac{b_s}{R}\left(1 + \frac{b_w}{b_s}\frac{t_w}{t_s}\right) \tag{21}$$

The weight equivalent solid plate thickness of the grid-stiffened shell $\bar{t}$ is readily calculated as

$$\frac{\bar{t}}{R} = \frac{t_s}{b_s}\frac{b_s}{R}\left(1 + 2\frac{b_w}{b_s}\frac{t_w}{t_s}\right) \tag{22}$$

Equations (15, 16, and 22) and the condition of optimum design that $p_{cr_G} = p_{cr_L} = p$ constitute four equations involv-

ing seven parameters: p_{crL}, p_{crG}, $\bar{t}/R$, b_w/b_s, t_w/t_s, t_s/b_s, and b_s/R.

One equation involving p, $\bar{t}/R$, b_w/b_s, and t_w/t_s is possible and is sought because it will relate the pressure to the weight parameter $\bar{t}/R$. The number of geometric proportions to be optimized can be reduced to one, b_w/b_s or t_w/t_s, by setting equal the two local modes of instability. The remaining geometric parameter (either b_w/b_s or t_w/t_s) can be independently varied to optimize the relationship between p and $\bar{t}/R$. Accordingly, Eqs. (15, 16, and 22), combined with the foregoing condition for optimum design, resolve to the following efficiency equation:

$$\bar{t}/R = F(p/E)^{3/5} \tag{23}$$

where F, an efficiency factor, is given by

$$F = \left(1 + 2\frac{b_w}{b_s}\frac{t_w}{t_s}\right)\left\{\frac{3\{2 + (1+\mu)[(b_w/b_s)(t_w/t_s)]\}}{(b_w/b_s)^3(t_w/t_s)[4 + (b_w/b_s)(t_w/t_s)]} \times \frac{12(1-\mu^2)}{2^3 k_s \pi^2}\right\}^{1/5} \frac{1}{C^{2/5}} \tag{24}$$

Consistent with the initially outlined assumptions, the following equation for critical pressure for buckling the stiffening elements is written:

$$p_{cr}/E = 2k_w\pi^2 (R/b_w)^2(\bar{t}/t_w)(D_w/ER^3) \tag{25}$$

where $k_w \cong 0.500$ for the assumed boundary conditions and

$$D_w/ER^3 = (t_w/R)^3/12(1-\mu^2) \tag{26}$$

Equating the critical stresses in the two local modes of instability leads to the following relationship between b_w/b_s and t_w/t_s (taking $k_s = 2.00$):

$$(b_w/b_s)(t_w/t_s) = 2r\{1 + [1 + (1/r)]^{1/2}\} \tag{27}$$

where

$$r = [\tfrac{1}{2}(t_w/t_s)]^4$$

The efficiency factor F in Eq. (24) is then

$$F = \frac{0.636\, r^{1/10}}{C^{2/5}} \frac{\{1 + 4r[1 + [1 + (1/r)]^{1/2}]\}}{\{r[1 + [1 + (1/r)]^{1/2}]\}^{3/5}} \times \left\{\frac{1 + 1.3r[1 + [1 + (1/r)]^{1/2}]}{2 + r[1 + [1 + (1/r)]^{1/2}]}\right\}^{1/5} \tag{28}$$

where $\mu = 0.3$. Figure 3 is a chart of Eq. (28) showing F vs t_w/t_s. The efficiency factor is a minimum 1.88, at $t_w/t_s = 0.80$ for $C = 1.0$, but the curve's flatness in that region indicates that t_w/t_s can be significantly off-optimum design without severe weight penalty. Figure 4 shows the relationship between b_w/b_s and t_w/t_s [Eq. (27)] to achieve the efficiencies shown in Fig. 3.

The auxiliary equations necessary for design are derived from Eqs. (22) and (16):

$$t_s = \bar{t}/[1 + 2(b_w/b_s)(t_w/t_s)] \tag{29}$$

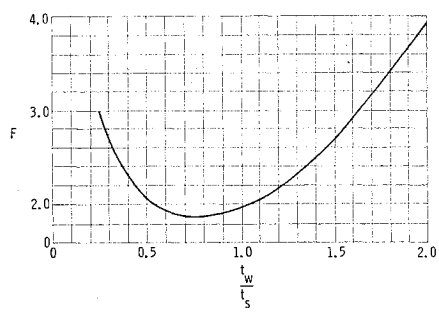

Fig. 3 Efficiency factor F for grid-stiffened domes, $\bar{t}/R = F(p/E)^{3/5}$, $C = 1$.

$$b_s = [3.62\, E\, t_s^3/pR]^{1/2} \tag{30}$$

Efficiency equation (23) is plotted in Fig. 5 for the minimum value of F, along with that for a monocoque shell. The buckling strength of the monocoque shell is taken as one-half its strength as predicted by classical theory (p. 517 of Ref. 9) to form a basis for comparison. This basis represents typical buckling pressures (middle of the wide scatter band) for deep monocoque shells of moderate R/t ratios.[12] Figure 5 shows the significant weight difference between these two types of construction.

Optimization of Size of Spherical Segment Dome

There is usually no compelling reason for being restrained to a hemispherical common dome. The following part of this minimum weight analysis is therefore given to form a basis for selecting an optimum spherical segment to form the compression dome. Figure 6 shows the nomenclature for the following analysis where the cylinder enclosing the dome is assumed to have a specified radius R_0. The problem is one of selecting the appropriate spherical dome radius R.

Assume that the entire radial reaction N_0 to the compressive pressure must be borne by a ring stressed to its tensile yield strength F_{ty}. The ring's cross-sectional area A_R is then

$$A_R = \frac{pR_0^2[1 - (R_0/R)^2]^{1/2}}{2F_{ty}(R_0/R)} \tag{31}$$

The ring's total weight W_R is then expressed in the form

$$\frac{W_R}{\rho_s R_0^3} = \pi \frac{p}{E}\frac{\rho_R}{\rho_s}\frac{E}{F_{ty}}\frac{[1 - (R_0/R)^2]^{1/2}}{R_0/R} \tag{32}$$

where ρ_R is the density of the ring material and ρ_s is the density of the shell material.

The weight of the spherical shell segment W_s is

$$\frac{W_s}{\rho_s R_0^3} = 2\pi \frac{\bar{t}}{R}\frac{\{1 - [1 - (R_0/R)^2]^{1/2}\}}{(R_0/R)^3} \tag{33}$$

The weight factor $\bar{t}/R$ is dependent only on the pressure-to-modulus ratio p/E and an efficiency factor F, and that dependence can be taken either from the present source or others for other details of geometry; in general, the relationship is

$$\bar{t}/R = F(p/E)^n \tag{34}$$

Total weight W_T of the ring-shell structure becomes

$$\frac{W_T}{\rho_s R_0^3} = \pi \frac{p}{E}\frac{\rho_R}{\rho_s}\frac{E}{F_{ty}}\frac{[1 - (R_0/R)^2]^{1/2}}{R_0/R} + 2\pi F\left(\frac{p}{E}\right)^n \frac{\{1 - [1 - (R_0/R)^2]^{1/2}\}}{(R_0/R)^3} \tag{35}$$

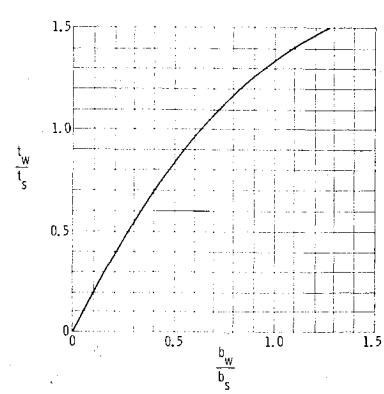

Fig. 4 Relationship between t_w/t_s and b_w/b_s for efficiencies shown in Fig. 3.

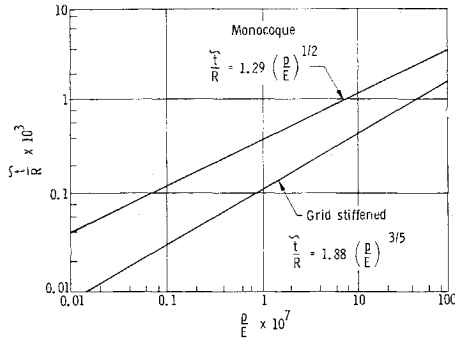

Fig. 5 Structural efficiency of monocoque and grid-stiffened spherical shells subjected to uniform crushing pressure ($C = 1$).

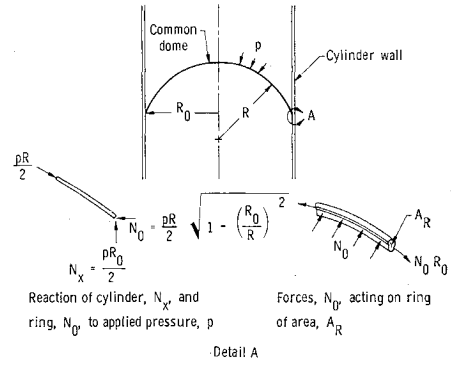

Fig. 6 Spherical segment common dome compressed by uniform pressure.

In this form, the total weight may be minimized by differentiating only with respect to the radius ratio R_0/R, since all other quantities are specified. The resulting expression for the optimum value is

$$R_0/R|_{\text{opt}} = (3 + 6B)^{1/2}/(2 + B) \tag{36}$$

where

$$B = (\rho_R/\rho_s)\ (E/F_{ty})\ (1/2F)\ (p/E)^{1-n}$$

For a case in which grid-stiffening is used where $F = 2.00$, $\rho_R = \rho_s$, $E = 10^7$ psi, $F_{ty} = 4 \times 10^4$ psi, and $p = 40$ psi,

$$R_0/R|_{\text{opt}} = 0.9726$$

This optimum configuration would weigh 93.5% of a hemispherical grid-stiffened dome for which (it is assumed) no ring is required.

For another case where the attachment ring is specified by other design requirements which, incidently, satisfies the "kick load" requirement, the optimum value of R_0/R is 0.866 and is independent of the shell efficiency. The shell weight in this case is 77% of that for a hemisphere having equal capability for carrying pressure.

Actual optimum designs would fall somewhere between the foregoing two extreme cases, since a large portion of the ring will be specified by other design requirements that are independent of the "kick loading" N_0.

Conclusions

Figure 5 shows clearly the high theoretical efficiency of grid-stiffened spherical shells for carrying crushing pressure. In practical ranges of application, efficiently designed grid-stiffened domes would weigh only 30–40% of the monocoque domes they would replace. Practical limitations of fabrication and layout of grid-stiffening patterns will lead to some compromise of that advantage, but the difference is expected to remain significant. The appropriate size spherical segment forming the dome is shown to depend on the requirements for the attachment ring. For all cases, however, the optimum segment is found to be less than a full hemisphere.

Even though the evidence presented tends to justify use of small deflection theory for predicting general instability of stiffened shells, the question will be resolved only by carefully planned experimentation. Such experimentation is recommended along with further analytical work to account for effects of one-sidedness on general instability.

References

[1] Donnell, L. H. and Wan, C. C., "Effect of imperfections on buckling of thin cylinders and columns under axial compression," J. Appl. Mech. **17**, 73–85 (March 1950).

[2] Donnell, L. H., "Stability of thin-walled tubes under torsion," NACA Rept. 479 (1933).

[3] Van der Neut, A., "The general instability of stiffened cylindrical shells under axial compression," National Aerospace Research Institute, Amsterdam, Rept. 5.314 (1947).

[4] Card, M. F., "Preliminary results of compression tests on cylinders with eccentric longitudinal stiffeners," NASA TM X-1004 (September 1964).

[5] Batdorf, S. B., "A simplified method of elastic-stability analysis for thin cylindrical shells," NACA Rept. 874 (1947).

[6] Zahorski, A., "Effects of material distribution on strength of panels," J. Aeronaut. Sci. **2**, 247–253 (1944).

[7] Farrar, D. J., "Design of compression structures for minimum weight," J. Roy. Aeronaut. Soc. **47**, 1041–1052 (1949).

[8] Crawford, R. F. and Burns, A. B., "Strength, efficiency and design data for beryllium structures," Aeronautical Systems Division ASD TR 61-692, Wright Patterson Air Force Base (1962).

[9] Timoshenko, S. and Gere, J., *Theory of Elastic Stability* (McGraw-Hill Book Co., Inc., New York, 1961), 2nd ed.

[10] Nickell, E. H. and Crawford, R. F., "Optimum ring stiffened cylinders subjected to uniform hydrostatic pressure," Society of Automotive Engineers Preprint 578F (1962).

[11] Crawford, R. F. and Libove, C., "Shearing effectiveness of integral stiffening," NACA TN 3443 (1955).

[12] Homewood, R. H., Brine, A. C., and Johnson, A. E., "Buckling instability of monocoque shells," Avco TR RAD-TR-9-59-20 (August 1959).

[13] Becker, H. and Gerard, G., "Elastic stability of orthotropic shells," J. Aerospace Sci. **29**, 505 (1962).

[14] Crawford, R. F. and Holmes, A. M. C., "RIFT interstage structural development program," Structures Study 1017, Lockheed Missiles and Space Co. (June 1962).

[15] Eakin, E., "Honeycomb cylinder tests," Douglas Aircraft SM-37719 (1961).

[16] Tennyson, R. C., "A note on the classical buckling load of circular cylindrical shells under axial compression," AIAA J. **1**, 475–476 (1963).